Malignant cells facilitate lung metastasis by bringing their own soil

Dan G. Duda[a,1], Annique M. M. J. Duyverman[a,1], Mitsutomo Kohno[a,1,2], Matija Snuderl[b], Ernst J. A. Steller[a,3], Dai Fukumura[a,4], and Rakesh K. Jain[a,4]

[a]Edwin L. Steele Laboratory for Tumor Biology, Department of Radiation Oncology, and [b]Department of Pathology, Massachusetts General Hospital and Harvard Medical School, Boston, MA 02114

Contributed by Rakesh K. Jain, October 30, 2010 (sent for review September 29, 2010)

Metastatic cancer cells (seeds) preferentially grow in the secondary sites with a permissive microenvironment (soil). We show that the metastatic cells can bring their own soil—stromal components including activated fibroblasts—from the primary site to the lungs. By analyzing the efferent blood from tumors, we found that viability of circulating metastatic cancer cells is higher if they are incorporated in heterotypic tumor–stroma cell fragments. Moreover, we show that these cotraveling stromal cells provide an early growth advantage to the accompanying metastatic cancer cells in the lungs. Consistent with this hypothesis, we demonstrate that partial depletion of the carcinoma-associated fibroblasts, which spontaneously spread to the lung tissue along with metastatic cancer cells, significantly decreases the number of metastases and extends survival after primary tumor resection. Finally, we show that the brain metastases from lung carcinoma and other carcinomas in patients contain carcinoma-associated fibroblasts, in contrast to primary brain tumors or normal brain tissue. Demonstration of the direct involvement of primary tumor stroma in metastasis has important conceptual and clinical implications for the colonization step in tumor progression.

Metastasis is a multistep process in which metastatic cancer cells must invade the surrounding stroma, intravasate, survive in the circulation, arrest, extravasate, invade the matrix, and grow in the target organ—all while evading destruction by the immune system (1).

One possible mechanism by which metastatic tumors may create a "congenial" soil in the secondary site and facilitate growth in the new organ environment is to prepare a "premetastatic site" by tumor-secreting factors (2–4). We have previously shown that "passenger" stromal cells contained in the original tumor source survive and proliferate during the initial growth of tumor fragments implanted in a new host (5). Here, we propose that the metastatic tumor cells bring passenger stromal cells from the primary tumor to the secondary site in the same host to provide a provisional stroma and facilitate initial growth and metastasis formation.

Studies reported more than 30 y ago showed that cancer cell clumping in circulation increases metastasis (6, 7). These clumps may be emboli, formed in circulation owing to interactions with immune cells (8–10). Indeed, injection of emboli containing both tumor and nontumor cells increases the efficiency of metastasis (6, 11). To test the hypothesis that metastatic cancer cells can bring their own soil to form metastases, we set out to answer five sequential questions. Do metastatic tumors shed heterotypic tumor fragments, and if so, is the viability of circulating cancer cells higher in heterotypic fragments? Could stromal cells in heterotypic fragments survive, proliferate, and facilitate early metastatic growth in the lungs? What type of stromal cells from the primary tumors could be detected in metastases spontaneously formed after primary tumor resection? Could the selective depletion of primary tumor-derived stromal cells—after resection of primary tumors—affect the spontaneous metastasis formation? And last, are primary tumor-associated stromal cells present in metastatic tumors in patients?

Results

Viability of Circulating Metastatic Cancer Cells Is Higher in Heterotypic Tumor Fragments. Tumors shed both single cells as well as clumps into the blood circulation. To establish whether the circulating clumps (circulating fragments consisting of at least two cancer cells) contain tumor-derived stromal cells (e.g., fibroblasts, endothelial, or tumor-infiltrated myeloid cells), we first implanted ds-Red–expressing metastatic Lewis lung carcinoma cells (LLC1) under the renal capsule in mice ubiquitously expressing the GFP—*Actb-GFP*/C57BL/6 mice, referred to hereafter as *Actb-GFP* mice. When tumors reached 9 to 10 mm in diameter, we performed an isolated tumor perfusion to collect and analyze the content of the efferent blood from the tumor (12, 13) (Fig. 1*A*). The vast majority (≈81%) of the shed ds-Red$^+$ cancer cells were single cells (Fig. 1*B*). However, we also collected small tumor clumps (≤200 μm in diameter) and all tumor clumps composed of six or more cells contained GFP-expressing host cells (Fig. 1 *B* and *C* and Table S1). In addition, activation of caspases 3 and 7—a measure of apoptosis—was detectable in most (≈88%) of the single or doublets of cancer cells at the time of shedding. In contrast, the heterotypic cell clumps contained almost twice as many viable cancer cells ($22.8 \pm 4.5\%$, $P < 0.05$; Fig. 1*D*).

Tumor Fragments May Increase Early Metastatic Tumor Growth by Carrying over Primary Tumor Stroma in the Lungs in an Experimental Metastasis Model. Clumps of cancer cells exhibit increased metastatic efficiency, even when viable cells are clumped with dead cells (7). Thus, we first sought to determine whether the host-derived passenger cells survive in circulation and are involved in metastatic tumor growth in the lungs. To this end, we i.v. injected in wild-type non-GFP C57BL/6 mice fluorescent tumor fragments (40–100 μm in diameter) obtained by mechanical dissociation of ds-Red-LLC1 tumors grown in *Actb-GFP* mice. In this experimental metastasis model, GFP$^+$ host-derived passenger cells survived and were detectable in ds-Red$^+$ lung metastatic nodules after 2 wk, as determined by whole-mount fluorescence microscopy (Fig. 2*A*). Similar results were obtained using another metastatic lung carcinoma line (LA-P0297) and syngeneic *EF1α-GFP*/FVB mice. Whereas not all initial micrometastatic foci eventually formed

Author contributions: D.G.D., A.M.M.J.D., M.K., D.F., and R.K.J. designed research; D.G.D., A.M.M.J.D., M.K., M.S., and E.J.A.S. performed research; R.K.J. contributed new reagents/analytic tools; D.G.D., A.M.M.J.D., M.K., M.S., E.J.A.S., D.F., and R.K.J. analyzed data; and D.G.D., A.M.M.J.D., D.F., and R.K.J. wrote the paper.

The authors declare no conflict of interest.

Freely available online through the PNAS open access option.

[1]D.G.D., A.M.M.J.D., and M.K. contributed equally to this work.

[2]Present address: Department of Surgery, Keio University School of Medicine, 35 Shinanomachi, Shinjuku-ku, Tokyo 160-8582, Japan.

[3]Present address: Department of Surgery, University Medical Center Utrecht, P.O. Box 85500, 3508 GA, Utrecht, The Netherlands.

[4]To whom correspondence may be addressed. E-mail: jain@steele.mgh.harvard.edu or dai@steele.mgh.harvard.edu.

This article contains supporting information online at www.pnas.org/lookup/suppl/doi:10.1073/pnas.1016234107/-/DCSupplemental.

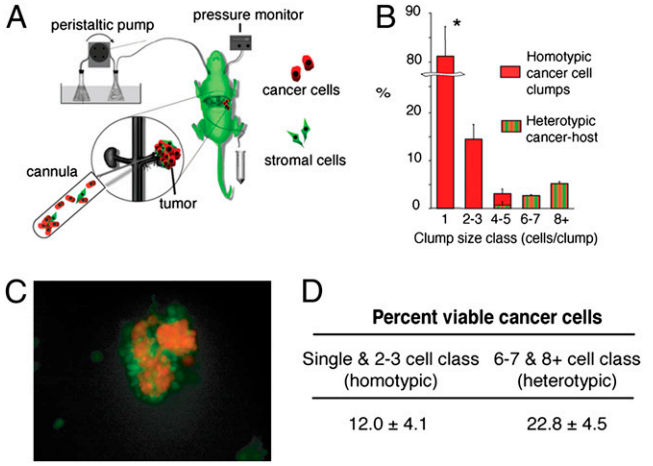

Fig. 1. Tumors shed fragments containing viable cancer cells in blood circulation. (*A*) Schema of the tumor perfusion and blood collection setup: ds-Red-LLC1 tumors were grown in the kidney of mice ubiquitously expressing GFP, and tumor perfusate was collected by cannulating the efferent vein (renal vein). (*B*) Histogram of the composition of shed tumor cells/clumps obtained from the renal perfusion experiment ($n = 5$ mice). The majority of shed cancer cells were single or doublets. Host-derived GFP$^+$ cells were present in all large clumps consisting of more than four to five cells. *$P < 0.05$. (*C*) Representative fluorescence multiphoton laser-scanning microscopy image of a heterogeneous clump, shed by a tumor using the isolated renal perfusion model. Green: stromal cells; red: tumor cells. (*D*) Viability of the shed cells and clumps using caspase staining: more than 22% of the ds-Red$^+$ cancer cells within heterotypic (cancer plus host cells) clumps were negative for caspase 3 and 7, whereas only 12% of the cancer cells collected as single cells or in homotypic clumps were viable ($P < 0.05$). Data are expressed as mean ± SD of four independent experiments.

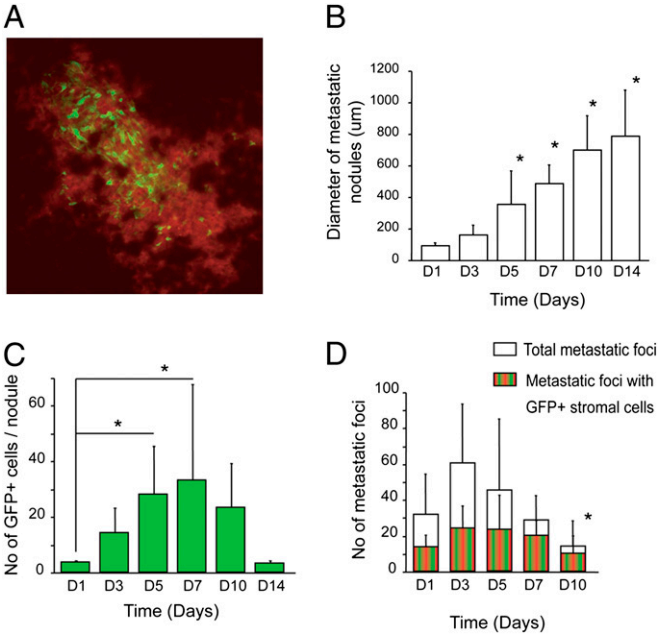

Fig. 2. Passenger stromal cells survive and promote initial growth after i.v. infusion of tumor fragments. (*A*) Multiphoton microscopy image (630 μm across) of GFP$^+$ primary tumor-derived stromal cells in a lung metastatic nodule in a C57BL/6 mouse 1 wk after i.v. infusion of *DsRed*-LLC1 tumor clumps obtained from a tumor growing in an *Actb-GFP* mouse. (*B*) Mean diameter of metastatic nodules increased significantly over time (*$P < 0.05$ vs. day 1). (*C*) Number of GFP$^+$ cells per metastatic nodule significantly increased from day 1 to days 5–7 (*$P < 0.05$ vs. day 1, $n = 4$–5 mice). GFP$^+$ cells are detectable for up to 2 wk in the macroscopic metastases. (*D*) Presence of GFP$^+$ host cell in the initial metastases seems to provide a growth advantage: the ratio of foci with host cells increases from ≈40% on day 1 to 70–80% around day 7–10 (*$P < 0.05$ vs. day 1). After day 10, there is a "dilution" in GFP$^+$ stromal cells (a decrease of the ratio to 35%), likely due to infiltration of the foci by non-GFP host-derived stromal cells.

established metastases, a substantial number of metastatic nodules formed over first 2 wk, and their mean diameter increased progressively (Fig. 2*B*). Of interest, the number of GFP$^+$ host-derived cells per nodule (in nodules that contained GFP$^+$ cells) increased significantly over the first 7 d of growth (Fig. 2*C*). Moreover, whereas the number of metastatic foci decreased with time, number of foci with GFP$^+$ host cells remained constant. As a result, at day 7, the fraction of metastatic nodules that contained GFP$^+$ stromal cells became significantly higher compared with that of the initial foci formed at day 1 after i.v. injection of the fragments (Fig. 2*D*). These data indicate that stromal cells associated with the primary tumor are involved in the metastatic nodules and survive and proliferate at the secondary site during early growth of metastatic foci. They also suggest that metastatic foci that contain primary tumor-derived stromal cells have a survival advantage.

Stromal Cells from Primary Tumors Are Detectable in Metastatic Nodules Spontaneously Formed in the Lungs After Primary Tumor Resection. To characterize the stromal cells that spontaneously "metastasize" with cancer cells, we adapted a parabiosis mouse model (14) to create a mouse with a 2-cm graft of GFP$^+$ skin and s.c. tissue. This procedure allowed us to generate a primary tumor with a rich GFP$^+$ stromal cell infiltration in a wild-type (non-GFP) C57BL/6 mouse (Fig. 3 *A*–*C* and *Materials and Methods*). We transplanted non-GFP LLC1 tumor cells in the GFP$^+$ skin and allowed the tumor to reach a diameter of 8 mm before resection. Three weeks after primary tumor resection, we studied grossly apparent lung metastases (arising from spontaneous foci formed before resection). In concert with the variability in GFP$^+$ cell number in the primary tumors, GFP$^+$ cells (i.e., primary tumor stroma-derived cells) were detectable in 27–86% of lung metastases. We used several different markers to characterize the GFP$^+$ cells by immunohistochemistry, given the known lack of marker specificity for stromal cells. We detected colocalization of GFP with expression of α-smooth muscle actin (αSMA) in 80% and of fibroblast-specific protein 1 (FSP1) in 75% of the stromal cells carried over to the lungs—both are indicative of the mesenchymal lineage (Fig. 3 *D* and *E*). In contrast, colocalization of GFP with F4/80 (a macrophage-selective marker) was detectable in 28% of the stromal cells.

Fibroblasts Carried over from the Primary Tumor Increase the Efficiency of Lung Metastasis. Because fibroblasts were highly prevalent among the traveling stromal cells detectable in metastases, we next tested whether their selective depletion in metastatic foci affects the metastatic growth. To this end, we used human carcinoma-associated fibroblasts (CAFs) and diphtheria toxin (DT) treatment (Fig. S1), because human cells are 1,000 times more sensitive to DT than murine cells and can be depleted by DT in vivo in mice (15, 16). We first grew tumors by coimplantation of LLC1 cells with human CAFs in SCID mice. CAFs persisted in the growing tumors (Fig. 4*A*) but did not affect their growth rate (Fig. S2*A*). However, CAF depletion with DT treatment resulted in a significant growth delay in primary tumors (Fig. S2*B*). To specifically deplete the CAFs that colonized the lungs, we systemically administered DT after primary tumor resection. The spontaneous colonization of the implanted CAFs to the lungs was confirmed by immunostaining. To this end, we used two antibodies specific for human antigens (that do not cross-react with either mouse fibroblasts or tumor cells) in lung tissues collected 3 d after amputation of the hindlimb bearing the tumor (Fig. 4 *B* and *C*).

In separate experiments, to specifically deplete the CAFs that colonized the lungs, we systemically administered DT to the

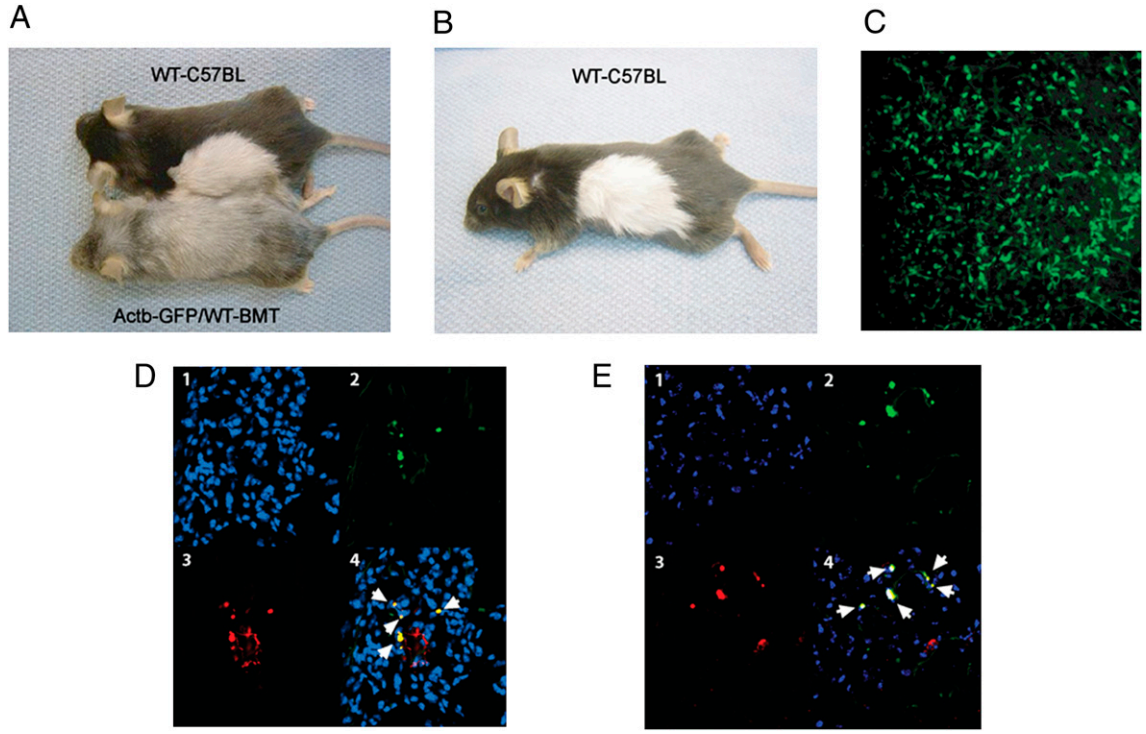

Fig. 3. Characterization of passenger stromal cells in a spontaneous metastasis formation model. (*A* and *B*) Transient parabiosis and BMT. (*A*) Transient parabiosis model using C57BL/6 and *Actb-GFP*/WT-BMT mice. (*B*) Fur depigmentation in *Actb-GFP*/WT-BMT mouse is secondary to the whole-body irradiation. (*C*) Representative multiphoton microscopy image of an LLC1 tumor grown in a successful GFP^+ skin graft transplanted in a WT-C57BL mouse. The image is 630 μm across. (*D* and *E*) Phenotypic analysis of GFP^+ primary tumor-derived stromal cells in metastases by immunohistochemistry and confocal microscopy: GFP^+ cells frequently express αSMA (white arrows in *D*) and FSP1 (*E*). The subpanels are (1) blue, DAPI nuclear stain; (2) green, GFP; (3) red, Cy3-labeled antibody staining; and (4) merged image. Images are 280 μm across.

tumor-bearing mice 1 d after complete resection of the primary tumors. DT treatment after resection significantly increased the survival compared with control (PBS) treatment ($P < 0.05$; Fig. 4*D*), but only in mice in which the primary tumors were generated by coimplantation of LLC1 with CAFs and not in mice implanted with LLC1 cells alone (Fig. S3). Moreover, when evaluated 2 wk after resection, the lungs of DT-treated mice contained significantly fewer macroscopic metastases than those of mice treated with PBS ($P < 0.05$; Fig. 4*E*). We confirmed the decrease in number of metastatic nodules after CAF depletion after resection using LA-P0297, another metastatic lung carcinoma cell line (Fig. 4*E*). Finally, we sought to determine whether CAF presence within the metastatic foci was critical for their promotion of metastatic growth. To this end, we i.v. injected single-cell suspensions containing LLC1 and CAFs, a model in which cells randomly distribute throughout the lung terminal capillaries and venules. We depleted the CAFs by DT treatment at 24 h after cell infusion. There was no significant difference in the number of metastases evaluated 2 wk after infusion (Fig. S4). These data show that tumor-associated fibroblasts can promote lung metastasis and that this promotion may not occur when the CAFs are not in direct association with the cancer cells within metastatic foci.

Tumor-Associated Fibroblasts Are Detectable in Human Carcinoma Metastases to the Brain, but Not in Primary Brain Tumors. We next sought to establish clinical relevance of the primary tumor-associated fibroblasts in metastasis. To this end, we examined brain metastases of patients with a variety of tumors. Brain metastasis is an ideal setting to detect primary tumor-derived stromal cells such as CAFs because normal brain tissue does not contain fibroblasts. We performed immunostaining for αSMA in human samples of brain metastases from carcinomas of the lung, breast, kidney, or endometrium and used normal brain and primary malignant brain tumors (i.e., glioblastoma) as a control. The only cells that stained positive for αSMA in normal brain and glioblastoma tissues were blood vessel-associated pericytes and smooth muscle cells (Fig. 5*A*). In contrast, we frequently detected benign-appearing $αSMA^+$ stromal cells with typical fibroblast spindle shape appearance distributed focally within the brain metastases in the extravascular area of the vast majority of cases (Fig. 5 *B–E*). Moreover, we detected by immunohistochemistry $CD10^+$ cells—a specific marker of endometrial stroma—in a rare case of endometrial carcinoma metastasis to the brain (Fig. 5*F*). Collectively these results provide compelling evidence for the presence and potential direct involvement of primary tumor-associated stromal cells in metastasis in cancer patients.

Discussion

Recent studies have shown that the efficiency of the metastatic process may be increased by various factors related to host-derived stroma. In experimental metastasis models, it has been shown that metastatic cells could lodge in the lungs before their oncogenic transformation (17) or could home to sites where immune cells or fibrocytes accumulate and promote metastatic growth (2–4, 18). It has also been shown that metastatic cells could form intravascular colonies in the lungs and subsequently invade the organ (19). In addition, there is mounting evidence that the stromal compartment plays an important role in tumor progression and metastasis. Previously it has been known that cancer cell clumping in circulation increases the metastasis efficiency. Here we show that host-derived stromal cells can directly contribute to the lung metastasis when carried over from the primary site within tumor fragments. Our data indicate that tumor-associated stromal cells shed from the primary tumor together with accompanying cancer

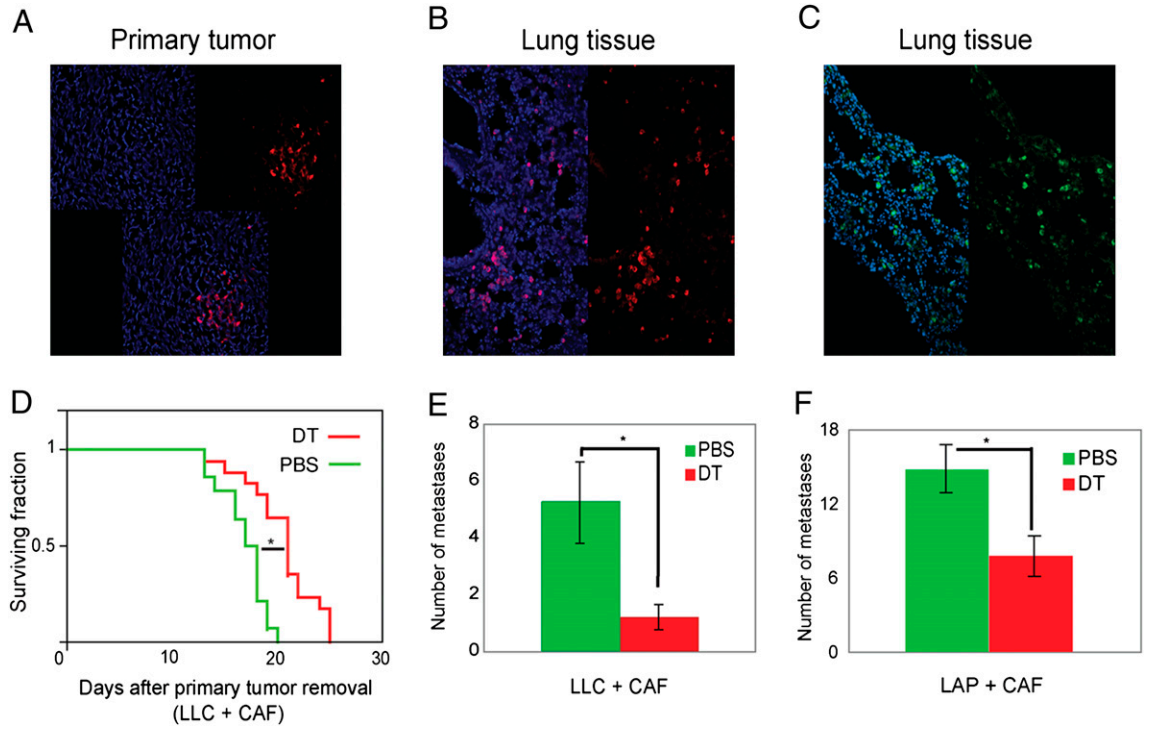

Fig. 4. Carryover of primary tumor stromal cells in lung metastases increases metastasis formation and survival. (*A–C*) Representative confocal microscopy images of primary tumors generated by coimplatation of human CAFs with LLC1 cells, confirming the persistence of CAFs in 5-mm tumors (*A*), as well as CAF presence in the lungs after primary tumor resection (*B* and *C*). Blue: DAPI nuclear stain; red: Cy3-labeled anti-human vimentin; green: FITC-labeled anti-human HLA. Images are 700 μm across. (*D*) Survival in mice with LLC1 metastases. CAF depletion using systemic DT treatment after tumor resection significantly increased survival (*$P < 0.001$ vs. PBS control, $n = 11–17$ mice). (*E* and *F*) CAF depletion by DT treatment after tumor resection significantly reduced the number of spontaneous macrometastases in (*E*) LLC1 (LLC) and (*F*) LA-P0297 (LAP) models (*$P < 0.05$ vs. PBS control, $n = 11–12$ mice).

cells survive in blood circulation as well as the secondary site and proliferate within the metastatic nodules. Preexistence of a tissue-like structure containing fibroblasts in clumps may increase the viability of cancer cells in blood circulation and the secondary site. In addition, these cells may support angiogenesis of metastatic nodules because CAFs express proangiogenic genes, including VEGF (Table S2). Although fibroblasts were highly prevalent among the traveling stromal cells, other potential passenger cells (e.g., monocytes/macrophages or lymphocytes, endothelial cells, etc.) may also promote metastasis. The roles of traveling stromal cells are likely to be more significant at the early stage of metastatic foci growth because their participation may be transient (5). By selective depletion of codisseminating CAFs of human origin, we demonstrate that this unique mechanism of metastatic cell colonization in the lungs can increase cancer's metastatic efficiency. Future studies should further evaluate the prevalence of this mechanism of metastasis in syngeneic and spontaneous animal models.

The ectopic presence of tumor-associated fibroblasts in brain metastases in patients indicates a potential clinical relevance of this phenomenon, which should also be explored further in future studies. It would be of great interest to demonstrate whether and how neoadjuvant (preoperative) therapies of primary tumors affect this process and whether evaluating circulating tumor clumps could complement circulating tumor cells studies. In particular, identifying the adhesion molecules that are responsible for the adherence between the cancer cells and fibroblasts may provide new targets for antimetastasis therapy. In what aspect this mechanism contributes to the organo-tropism of certain metastatic tumors is also unclear. Nevertheless, demonstration of the possible involvement of the same tumor "soil" in both local and distant lesions has important conceptual implications for the colonization step of metastatic cascade.

Materials and Methods

Cells and Gene Transfections. We used two cell lines with established metastatic potential: Lewis lung carcinoma (LLC-1) and LA-P0297 (20–22). All cells were maintained in DMEM supplemented with 10% FBS. For some of the experiments, the cancer cells were transfected with *dsRed* using a retroviral vector [pMOWSdSV4.0-DsRED express, a kind gift from Dr. Brian Seed, Massachusetts General Hospital (MGH), Boston, MA]. CAFs and the CAF isolation protocol were generously provided by Dr. R. Weinberg (Massachusetts Institute of Technology, Cambridge, MA). See details in *SI Materials and Methods*.

Animals. C57BL/6 mice expressing GFP under the chicken β-actin promoter and CMV enhancer (*Actb-GFP*) were purchased from Jackson Laboratories and then rederived, bred, and maintained in our animal facility. Wild-type (non-GFP) C57BL/6 and SCID mice were also bred and maintained in our gnotobiotic animal facility. All animal procedures were performed according to the guidelines of Public Health Service Policy on Humane Care of Laboratory Animals and in accordance with an approved protocol by the Institutional Animal Care and Use Committee of MGH.

Tumor Perfusion and Efferent Blood Collection. Male *Actb-GFP* mice, 6–10 wk of age, were used for a kidney-isolated tumor perfusion model as previously described (12, 13). *DsRed*-LLC1 cells (1×10^6) were injected under the capsule of the kidney. Tumors were allowed to grow for 10–12 d. To collect shed cancer cells and clumps, the renal vein of the left kidney was cannulated, and 3 to 4 mL of perfusate was collected and passed through a polycarbonate membrane filter (8-μm pore size) (Sterlitech). Cytological elements retained on the filter were analyzed quantitatively by fluorescence multiphoton laser-scanning microscopy for the presence of ds-Red$^+$ cancer cells and GFP$^+$ host cells.

Apoptosis Assay. To evaluate the viability of shed cancer cells, we used the Carboxyfluorescein Caspase 3 FLICA (Immunochemistry Technologies) according to the manufacturer's protocol. C57BL/6 mice were inoculated with *DsRed*-LLC1 cells in the kidney, and the shed cells were collected as described above. We detected caspase 3 and 7 activities (detected as green fluorescence signal) by fluorescence confocal microscopy.

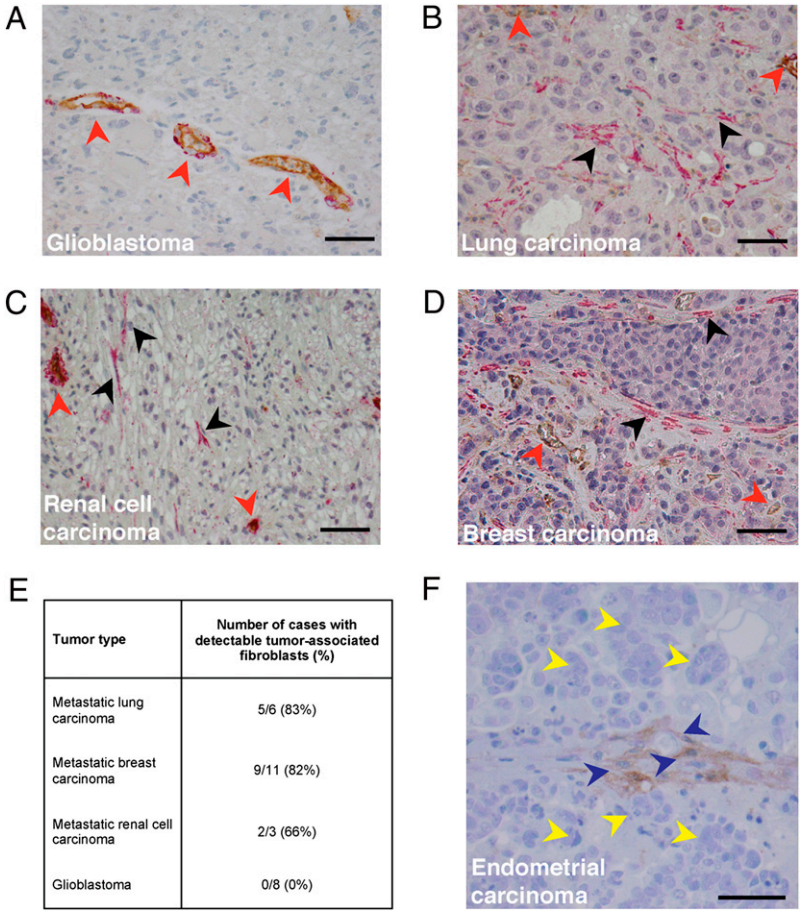

Tumor type	Number of cases with detectable tumor-associated fibroblasts (%)
Metastatic lung carcinoma	5/6 (83%)
Metastatic breast carcinoma	9/11 (82%)
Metastatic renal cell carcinoma	2/3 (66%)
Glioblastoma	0/8 (0%)

Fig. 5. Clinical evidence for carryover of primary tumor stromal cells in human metastases. (*A*) Representative microscopy image of glioblastoma tissue. Red arrowheads indicate tumor vessels after αSMA/CD31 double staining. In normal human brain and primary brain tumors, only vessel-associated pericytes and vascular smooth muscle cells are αSMA positive. (*B–D*) Representative microscopy images of human brain metastases originating from (*B*) lung carcinoma, (*C*) renal cell carcinoma, and (*D*) breast carcinoma. Red arrowheads indicate αSMA-positive perivascular cells associated with CD31-positive vascular endothelial cells. Black arrowheads indicate focal presence of αSMA-positive tumor-associated fibroblasts. (*E*) Quantification of cases of human brain metastasis with detectable tumor-associated fibroblasts. (*F*) Representative microscopy image of human brain metastasis from endometrial carcinoma: endometrial stromal cells ($CD10^+$ cells, blue arrowheads) are detectable in the brain in close association with the cancer cells (yellow arrowheads). (Scale bars, 50 μm.)

Experimental Lung Metastasis Using Tumor Fragment Infusion. Male SCID mice, 8–10 wk of age, were used for the experimental lung metastases model. *DsRed*-LLC1 tumors grown in *Actb-GFP* mice were mechanically dissociated and serially filtered through 100- and 40-μm cell strainers (BD Biosciences). Tumor fragments were recovered and infused in nontransgenic C57BL/6 mice at a concentration of ≈2,000–3,000 fragments per 0.4 mL i.v. On days 1, 3, 5, 7, 10, and 14 after tumor fragment infusion, lung metastases were counted on whole-tissue mounts. In all foci, the number of GFP^+ stromal cells was quantitatively analyzed in images captured by fluorescence multiphoton laser-scanning microscopy. This experiment was repeated using another lung carcinoma cell line, LA-P0297, and syngeneic FVB mice ubiquitously expressing GFP (*EF1α-GFP* transgenic mice).

Bone Marrow Transplantation. Restorative bone marrow transplantation (BMT) to mice that had been lethally irradiated using a dose of 2 × 6 Gy was performed as previously described (20).

Skin Graft from BMT Mice Through Parabiosis. To detect tumor host-derived cells in lung metastases, we engrafted *Actb-GFP* skin to a wild-type C57BL/6 mouse through the parabiosis procedure (i.e., by surgically conjoining the mice from the shoulder to the hip to share a common circulation). Two months before the surgical procedure, *Actb-GFP* received a restorative BMT from wild-type C57BL/6 mice (*Actb-GFP*/WT-BMT). The mice were kept in parabiosis with syngeneic C57BL/6 mice for 3 wk and then surgically separated. After surgery, a 2-cm flap of the skin and s.c. tissues were transferred from the *Actb-GFP*/WT-BMT mice and sutured on the C57BL/6 mice. Before s.c. tumor inoculation in these mice we confirmed (*i*) the absence of hematopoietic GFP^+ cells in circulation and in digested lung tissue by flow cytometry; and (*ii*) the lack of $αSMA^+GFP^+$ and $FSP1^+GFP^+$ cell presence in the lung tissues by flow cytometry and immunohistochemistry. One million LLC1 cells were s.c. inoculated in the engrafted skin area. Tumors were resected when they reached 8 mm in diameter, and primary tumors were analyzed for GFP^+ cell content. Because of significant incorporation of non-GFP cells in the primary tumors, the fraction of GFP^+ vs. non-GFP cells varied from mouse to mouse. Thus, for the phenotypic analysis, we included only the mice that had detectable levels of GFP^+ cell recruitment in the primary tumors (five of seven mice; 71%).

Spontaneous Lung Metastasis Formation After Primary Tumor Resection. Male SCID mice, 8–10 wk of age, were coimplanted s.c. with 2×10^5 LLC1 (or LA-P0729) tumor cells and 1×10^6 human CAFs in 0.1 mL of PBS (i.e., at a 1:5 ratio). For primary tumor growth experiments, tumors were allowed to grow to a size of 5 mm, before they were treated with 0.2 mL of 1 μg/mL DT (Sigma). In the spontaneous metastasis formation models, tumors were allowed to grow to a size of 10 mm before they were resected. One day after primary tumor resection, mice were treated with 0.2 mL of DT at a dose of 1 μg/mL or PBS as a control. In pilot studies, we found that systemic DT treatment at this dose was effective in delaying tumor growth after s.c. injection of CAFs with LLC1 cells but not after s.c. injection of LLC1 cells alone. Mice were killed when they showed signs of advanced disease (weight loss >15%, ruffled fur, and/or cachexia). Survival time distributions were analyzed using Kaplan–Meier plots. The number of macroscopic metastases per lung was counted using a dissecting microscope.

Tissue Preparation and Fluorescence Immunohistochemistry. Mice were perfusion fixed by with paraformaldehyde and incubated in sucrose before embedding. Frozen tissue sections (10–20 μm) were analyzed for endogenous GFP expression. We used antibodies against mouse F4/80, αSMA, and FSP1 (S100A4) for immunohistochemical characterization of stromal cells. For human CAF identification, tissues were immunostained with anti-human vimentin or HLA-ABC antigen antibodies. Tissues were mounted using DAPI containing mounting media. See details in *SI Materials and Methods*.

Immunohistochemical Analysis of Brain Metastases from Carcinoma and Glioblastoma Patients. Formalin-fixed paraffin-embedded brain tumor tissue from patients with glioblastoma, metastatic lung, breast, renal cell, and endometrial carcinoma were obtained from the Department of Pathology, MGH, Boston. Tissues were immunostained using a CD31/αSMA double-staining protocol or using anti-CD10 antibody. Tissues were counterstained with hematoxylin. *SI Materials and Methods*.

Quantification of Confocal Images. Colocalization of αSMA, FSP1, and F4/80 expression with GFP^+ in stromal cells was quantified using fluorescence confocal microscopy (n = 6 mice, five to six sections each). The size of all of the images analyzed was 1,024 × 1,024 pixels.

Statistical Analysis. Data are expressed as mean ± SEM, and statistical analysis was performed using the Student t test (two-tailed with unequal variance). For survival data analysis, we generated Kaplan–Meier plots (JMP, version 5.0.1.2; SAS), with failure defined as the need to kill animals because of signs of advanced metastatic disease. Statistical differences were calculated using log–rank test. For all analyses, a P value of <0.05 was considered statistically significant.

Note Added in Proof. While this article was being processed for publication, Xu et al. (23) reported data consistent with ours in a model of pancreatic cancer metastasis.

ACKNOWLEDGMENTS. We thank Drs. I. J. Fidler, Y. Izumi, and B. Seed for useful suggestions; L. Xu, K. S. Cohen, M. R. Dawson, N. Hosseini, P. Huang, J. Kahn, M. Kim, S. Roberge, and C. Smith for invaluable help with the experiments; and M. Ancukiewicz for statistical analysis. This study was performed with support provided by Grant R01CA085140 (to R.K.J.) and was partially supported by Grants P01CA080124, R01CA115767, R01CA126642 (all to R.K.J.), and R01CA096915 (to D.F.), all from the National Institutes of Health. A.M.M.J.D. received Department of Defense Fellowship W81XWH-06-1-0781. M.K. received a research fellowship from the Japanese Ministry of Health and Welfare.

1. Talmadge JE, Fidler IJ (2010) AACR centennial series: The biology of cancer metastasis: Historical perspective. *Cancer Res* 70:5649–5669.
2. Hiratsuka S, et al. (2002) MMP9 induction by vascular endothelial growth factor receptor-1 is involved in lung-specific metastasis. *Cancer Cell* 2:289–300.
3. Kim S, et al. (2009) Carcinoma-produced factors activate myeloid cells through TLR2 to stimulate metastasis. *Nature* 457:102–106.
4. Kaplan RN, et al. (2005) VEGFR1-positive haematopoietic bone marrow progenitors initiate the pre-metastatic niche. *Nature* 438:820–827.
5. Duda DG, et al. (2004) Differential transplantability of tumor-associated stromal cells. *Cancer Res* 64:5920–5924.
6. Liotta LA, Saidel MG, Kleinerman J (1976) The significance of hematogenous tumor cell clumps in the metastatic process. *Cancer Res* 36:889–894.
7. Fidler IJ (1973) The relationship of embolic homogeneity, number, size and viability to the incidence of experimental metastasis. *Eur J Cancer* 9:223–227.
8. Ruiter DJ, van Krieken JH, van Muijen GN, de Waal RM (2001) Tumour metastasis: Is tissue an issue? *Lancet Oncol* 2:109–112.
9. Fidler IJ (2003) The pathogenesis of cancer metastasis: The 'seed and soil' hypothesis revisited. *Nat Rev Cancer* 3:453–458.
10. Sahai E (2007) Illuminating the metastatic process. *Nat Rev Cancer* 7:737–749.
11. Updyke TV, Nicolson GL (1986) Malignant melanoma cell lines selected in vitro for increased homotypic adhesion properties have increased experimental metastatic potential. *Clin Exp Metastasis* 4:273–284.
12. Swartz MA, et al. (1999) Cells shed from tumours show reduced clonogenicity, resistance to apoptosis, and in vivo tumorigenicity. *Br J Cancer* 81:756–759.
13. Kristjansen PE, Roberge S, Lee I, Jain RK (1994) Tissue-isolated human tumor xenografts in athymic nude mice. *Microvasc Res* 48:389–402.
14. Wagers AJ, Sherwood RI, Christensen JL, Weissman IL (2002) Little evidence for developmental plasticity of adult hematopoietic stem cells. *Science* 297:2256–2259.
15. Arbiser JL, et al. (1999) Isolation of mouse stromal cells associated with a human tumor using differential diphtheria toxin sensitivity. *Am J Pathol* 155:723–729.
16. Padera TP, et al. (2004) Pathology: Cancer cells compress intratumour vessels. *Nature* 427:695.
17. Podsypanina K, et al. (2008) Seeding and propagation of untransformed mouse mammary cells in the lung. *Science* 321:1841–1844.
18. van Deventer HW, et al. (2008) C-C chemokine receptor 5 on pulmonary fibrocytes facilitates migration and promotes metastasis via matrix metalloproteinase 9. *Am J Pathol* 173:253–264.
19. Al-Mehdi AB, et al. (2000) Intravascular origin of metastasis from the proliferation of endothelium-attached tumor cells: A new model for metastasis. *Nat Med* 6: 100–102.
20. Duda DG, et al. (2006) Evidence for incorporation of bone marrow-derived endothelial cells into perfused blood vessels in tumors. *Blood* 107:2774–2776.
21. Huang P, Duda DG, Jain RK, Fukumura D (2008) Histopathologic findings and establishment of novel tumor lines from spontaneous tumors in FVB/N mice. *Comp Med* 58:253–263.
22. O'Reilly MS, et al. (1994) Angiostatin: A novel angiogenesis inhibitor that mediates the suppression of metastases by a Lewis lung carcinoma. *Cell* 79:315–328.
23. Xu Z, et al. (2010) Role of pancreatic stellate cells in pancreatic cancer metastasis. *American Journal of Pathology* 177:2585–2596.